VSP

Advanced Composite Materials 17 (2008) 301–317

ADVANCED COMPOSITE MATERIALS
www.brill.nl/acm

Evaluation Method of Adhesive Fracture Toughness Based on Double Cantilever Beam (DCB) Tests Including Residual Thermal Stresses

Tomohiro Yokozeki [a,*] **and Toshio Ogasawara** [b]

[a] Department of Aeronautics and Astronautics, University of Tokyo, 7-3-1 Hongo, Bunkyo-ku, Tokyo 113-8656, Japan

[b] Advanced Materials Group, Aerospace Research and Development Directorate, Japan Aerospace Exploration Agency, 6-13-1 Osawa, Mitaka, Tokyo 181-0015, Japan

Received 18 June 2007; accepted 25 January 2008

Abstract

The energy release rate associated with crack growth in adhesive double cantilever beam (DCB) specimens, including the effect of residual stresses, was formulated using beam theory. Because of the rotation of the asymmetric arms in the adhesive DCB specimens due to temperature change, it is necessary to correct the evaluated fracture toughness of the DCB specimens, specifically in the case of a large temperature change. This study shows that the difference between the true toughness and an apparent toughness due to the consequence of ignoring residual stresses can be calculated for a given specimen geometry and thermo-mechanical properties (e.g. coefficient of thermal expansion). The calculated difference in the energy release rates based on the present correction method is compared with that from FEM in order to verify the present correction method. The residual stress effects on the evaluation of the adhesive fracture toughness are discussed.

Keywords

Adhesives, fracture toughness, residual thermal stress

1. Introduction

The application of carbon fiber-reinforced plastic (CFRP) laminates to the cryogenic propellant tank structures has been widely attempted in order to achieve a drastic structural weight reduction of space launch vehicles. Because cryogenic liquefied fuels (e.g. liquid hydrogen, liquid oxygen and liquid natural gas) are expected to be used for high-performance space launch vehicles, the characterization of thermo-mechanical properties and fracture properties of CFRPs in the cryogenic

* To whom correspondence should be addressed. E-mail: yokozeki@aastr.t.u-tokyo.ac.jp
Edited by JSCM

DOI:10.1163/156855108X345207

environment is a key research topic [1, 2]. Recent researches on the applicability of CFRP laminates to cryogenic tank structures indicate that microscopic damage accumulation (i.e. matrix cracks) in CFRP laminates is inevitable due to severe thermo-mechanical loads, which causes a fuel leak problem through the microscopic damage networks [2, 3]. Therefore, the application of liners (e.g. metal liner) to the composite tank structures is attempted in order to prevent fuel leakage. For example, a cryogenic composite tank with an aluminum liner was developed for the tank of liquid natural gas propulsion system. However, some difficulties in the feasibility and the integrity of this tank were pointed out, such as the fact that metal–composite interface debondings are unavoidable due to thermal misfits and severe thermal loads. In addition, it is necessary to apply adhesive joints to the joining of the cryogenic tank and frame structures from the processing and leakage points of view. Fracture properties of the adhesive joints and effects of residual thermal stresses on the interface fracture toughness should be investigated for the design of adhesive joint structures. It is therefore important to evaluate the fracture mechanics properties of adhesive joints under cryogenic conditions [4–6].

One of the representative test methods for the characterization of adhesive fracture toughness is the double cantilever beam (DCB) test that is standardized in professional associations (e.g. ASTM) [7, 8]. Effects of residual thermal stresses should be incorporated when evaluating the fracture toughness of DCB specimens subjected to temperature change from the cure temperature. For example, consider the upper half of a DCB beam consisting of the adherend and the adhesive as shown in Fig. 1. When the adherend with a low coefficient of thermal expansion (CTE) is placed outside the adhesive with a high CTE, a bending deformation of the cracked arm is induced so that the arm eliminates the induced bending moment due to the thermal misfit. Therefore, the cracked arm deflects inside when subjected to a decrease in temperature, which may result in a decrease in the crack opening displacement. It is expected that the energy release rates will decrease even when

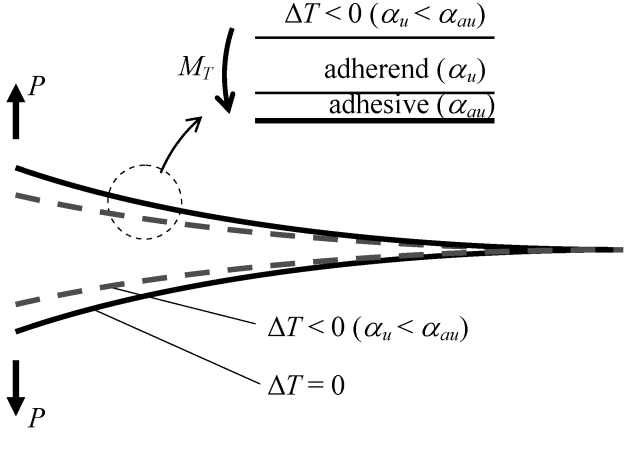

Figure 1. Thermally-induced bending moment in an adhesive DCB specimen.

the same load is applied to the specimen. In contrast, the energy release rates will increase in the cases of temperature increase or DCB specimens consisting of the adherend and the adhesive with the opposite relation of CTE. In addition, consider a DCB specimen with different adherends (asymmetric DCB specimen). Due to a temperature change, bending deformation is induced in the bonded region, and this deformation is eliminated in the cracked region. Thus, non-zero energy release rates exist in the DCB specimen without any applied load. The above-mentioned effects of residual thermal stresses on the evaluation of fracture toughness are not considered in the standards. These effects should be incorporated when evaluating the adhesive fracture toughness, specifically under cryogenic conditions.

Jiao *et al*. [9] described the effect of residual thermal stresses on the fracture toughness evaluation of asymmetric DCB specimens. They measured adhesive fracture toughnesses incorporating the thermal misfit between the different adherends. However, the adhesive layer was neglected in their study, and the thermal misfit between the adhesive and the adherends should be also included. Nairn [10] incorporated the effect of the adhesive layer into the evaluation of the adhesive fracture toughness of a symmetric DCB specimen with a central crack in the adhesive layer, and formulated the energy release rate including residual thermal stresses. In the actual DCB specimens and adhesive structures, there are many cases where the adhesive structures have asymmetric configurations (e.g. CFRP and metal joints) and interfacial cracks propagate between the adherends and the adhesive. Therefore, it is necessary to investigate and formulate effects of residual thermal stresses on the evaluation of adhesive fracture toughness in general adhesive configurations.

In this study, a general DCB specimen (e.g. different adherends, asymmetric crack position) is modeled as a laminated beam, and the energy release rate associated with the crack growth is formulated including residual thermal stresses. The relationship between the apparent fracture toughness (without considering thermal stresses) and the true fracture toughness is clarified, and a correction method of the evaluation of fracture toughness is presented. This correction method is verified by comparing it with FEM results. Discussions on the effect of residual thermal stresses on the energy release rates are provided.

2. Formulation of Energy Release Rate

2.1. Energy Release Rates Including Residual Thermal Stresses

The mechanical response of linear-elastic materials subjected to thermo-mechanical loads can be expressed as the superposition of the case subjected to mechanical loads (superscript m) and that subjected to temperature changes (superscript r). The energy release rate is expressed as

$$G = -\frac{\mathrm{d}\Pi}{\mathrm{d}A} = \frac{\mathrm{d}W}{\mathrm{d}A} - \frac{\mathrm{d}U}{\mathrm{d}A}, \tag{1}$$

where

$$U = \frac{1}{2}\int_V \boldsymbol{\sigma}\cdot(\boldsymbol{\varepsilon}-\boldsymbol{\alpha}\Delta T)\,\mathrm{d}V = \frac{1}{2}\int_V (\boldsymbol{\sigma}^{\mathrm{m}}+\boldsymbol{\sigma}^{\mathrm{r}})\cdot(\boldsymbol{\varepsilon}^{\mathrm{m}}+\boldsymbol{\varepsilon}^{\mathrm{r}}-\boldsymbol{\alpha}\Delta T)\,\mathrm{d}V,$$
$$W = \int_{S_{\mathrm{T}}} \tilde{\mathbf{T}}\cdot\mathbf{u}\,\mathrm{d}S = \int_{S_{\mathrm{T}}} \tilde{\mathbf{T}}\cdot(\mathbf{u}^{\mathrm{m}}+\mathbf{u}^{\mathrm{r}})\,\mathrm{d}S. \tag{2}$$

Here, $\boldsymbol{\sigma}$, $\boldsymbol{\varepsilon}$, $\boldsymbol{\alpha}$, $\mathbf{u}$ and $\tilde{\mathbf{T}}$ are stress tensor, strain tensor, CTE tensor, displacement vector and traction vector prescribed in traction boundary conditions, respectively. In these equations, ΔT is temperature change (difference between curing or stress-free temperature and operation temperature), A is crack area, V is volume and S_{T} is the traction-prescribed boundary area. In reference to Nairn's formulation [11], energy release rates of the cracked materials surrounded only by traction-prescribed boundaries (including temperature changes) are expressed as

$$G = \frac{\mathrm{d}}{\mathrm{d}A}\left(\frac{1}{2}\int_{S_{\mathrm{T}}} \tilde{\mathbf{T}}\cdot\mathbf{u}^{\mathrm{m}}\,\mathrm{d}S + \int_{S_{\mathrm{T}}} \tilde{\mathbf{T}}\cdot\mathbf{u}^{\mathrm{r}}\,\mathrm{d}S + \frac{1}{2}\int_V \boldsymbol{\sigma}^{\mathrm{r}}\cdot\boldsymbol{\alpha}\Delta T\,\mathrm{d}V\right). \tag{3}$$

The derivation of this equation is referred to Appendix A.

2.2. Energy Release Rate of DCB Specimen

Consider a DCB specimen as shown in Fig. 2. The energy release rate of this DCB specimen is derived using the beam theory and equation (3). The upper and lower regions of the cracked arm are referred to as region 1 and 2, and the uncracked region is denoted as region 3. These regions are expressed in the following equations as superscripts with parentheses. The displacement at the loading point due to the applied load P is denoted as δ (the upward direction corresponds to the positive direction). The equation (3) can be expressed as

$$\begin{aligned} G &= \frac{P}{2B}\frac{\mathrm{d}}{\mathrm{d}a}(\delta^{\mathrm{m}(1)}-\delta^{\mathrm{m}(2)}) + \frac{P}{B}\frac{\mathrm{d}}{\mathrm{d}a}(\delta^{\mathrm{r}(1)}-\delta^{\mathrm{r}(2)}) + \frac{1}{2B}\frac{\mathrm{d}}{\mathrm{d}a}\int_V \boldsymbol{\sigma}^{\mathrm{r}}\cdot\boldsymbol{\alpha}\Delta T\,\mathrm{d}V \\ &\equiv G^{\mathrm{app}} + \Delta G_a + \Delta G_b, \end{aligned} \tag{4}$$

where B is the specimen width and a is the crack length. The first term of equation (4) corresponds to the apparent energy release rate without considering residual thermal stresses, and the second and the third terms are correction terms including residual thermal stresses. Specifically, the second term expresses the correction of the effect of residual thermal deformation on the displacement at the loading point, and the third term corresponds to energy release rate associated with crack growth subjected only to temperature change. Note that geometric non-linearity is neglected herein.

The first and the second terms of equation (4) are considered at first. The displacement at the loading point due to the applied load P can be expressed as

$$\delta^{\mathrm{m}(1)} = \frac{1}{3}C^{(1)}Pa^3, \qquad \delta^{\mathrm{m}(2)} = -\frac{1}{3}C^{(2)}Pa^3 \tag{5}$$

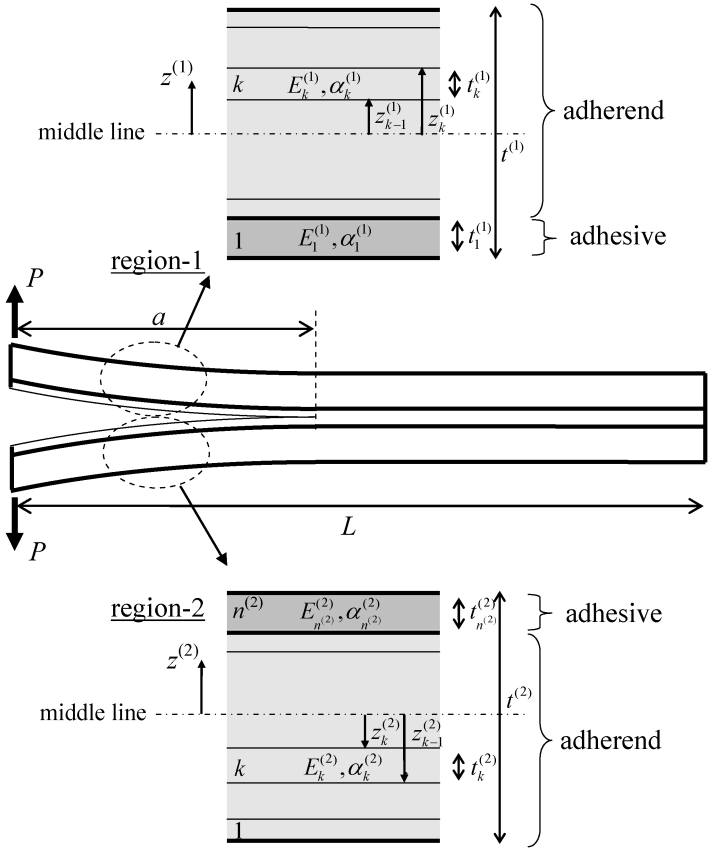

Figure 2. Adhesive DCB test specimen.

and the displacement subjected only to temperature change is expressed as

$$\delta^{\mathrm{r}(1)} = \frac{1}{2} F^{(1)} \Delta T a^2, \qquad \delta^{\mathrm{r}(2)} = \frac{1}{2} F^{(2)} \Delta T a^2 \tag{6}$$

using beam theory (see Appendix B). Here, C and F are the constants obtained from the lamination theory.

$$C^{(k)} = \frac{A_{11}^{(k)}}{A_{11}^{(k)} D_{11}^{(k)} - B_{11}^{(k)2}}, \qquad F^{(k)} = \frac{B_{11}^{(k)} N_{\mathrm{T}}^{(k)} - A_{11}^{(k)} M_{\mathrm{T}}^{(k)}}{A_{11}^{(k)} D_{11}^{(k)} - B_{11}^{(k)2}}, \tag{7}$$

$$A_{11}^{(k)} = B \sum_i E_i^{(k)} \left(z_i^{(k)} - z_{i-1}^{(k)} \right),$$

$$B_{11}^{(k)} = \frac{1}{2} B \sum_i E_i^{(k)} \left(z_i^{(k)2} - z_{i-1}^{(k)2} \right),$$

$$D_{11}^{(k)} = \frac{1}{3} B \sum_i E_i^{(k)} \left(z_i^{(k)3} - z_{i-1}^{(k)3} \right), \tag{8}$$

$$N_{\mathrm{T}}^{(k)} = B\sum_i E_i^{(k)}\alpha_i^{(k)}\big(z_i^{(k)} - z_{i-1}^{(k)}\big),$$

$$M_{\mathrm{T}}^{(k)} = \frac{1}{2}B\sum_i E_i^{(k)}\alpha_i^{(k)}\big(z_i^{(k)2} - z_{i-1}^{(k)2}\big).$$

In equations (7) and (8), E and α are Young's modulus and CTE in the longitudinal direction, respectively, $z^{(k)}$ is the position from the middle plane in the region k and subscript i denotes each layer. Because the beam theory neglects shear and extensional deformation in the thickness direction, the displacement at the loading point due to shear load P, equation (5), is usually corrected using the end correction parameter χ as shown in the following equation [12].

$$\delta^{\mathrm{m}(1)} = \frac{1}{3}C^{(1)}P(a + \chi^{(1)}t^{(1)})^3, \qquad \delta^{\mathrm{m}(2)} = -\frac{1}{3}C^{(2)}P(a + \chi^{(2)}t^{(2)})^3. \tag{9}$$

In this equation, $t^{(k)}$ denotes the total thickness of each region. In the case of temperature change, the induced deformations result from distributed moments and thus, equation (6) is considered to be accurate.

Next, consider the third term of equation (4). Because this term corresponds to the energy release rate associated with crack growth subjected only to temperature change, explicit derivation can be performed using lamination theory in the case of DCB specimens with a long crack compared with thickness (steady-state case). From the equation (B.4) in Appendix B, the residual thermal stresses in the laminated beam can be expressed as

$$\sigma_i^{\mathrm{r}(k)} = E_i^{(k)}\big(\varepsilon_0^{(k)} - \alpha_i^{(k)}\Delta T + z^{(k)}\kappa^{(k)}\big), \tag{10}$$

where

$$\begin{aligned}
\varepsilon_0^{(k)} &= \frac{D_{11}^{(k)}N_{\mathrm{T}}^{(k)} - B_{11}^{(k)}M_{\mathrm{T}}^{(k)}}{A_{11}^{(k)}D_{11}^{(k)} - B_{11}^{(k)2}}\Delta T \equiv H^{(k)}\Delta T,\\
\kappa^{(k)} &= \frac{A_{11}^{(k)}M_{\mathrm{T}}^{(k)} - B_{11}^{(k)}N_{\mathrm{T}}^{(k)}}{A_{11}^{(k)}D_{11}^{(k)} - B_{11}^{(k)2}}\Delta T \equiv -F^{(k)}\Delta T.
\end{aligned} \tag{11}$$

This equation corresponds to equation (B.9). Substituting equation (10) into the third term in equation (4),

$$\begin{aligned}
&\int_{V^{(k)}} \boldsymbol{\sigma}^{\mathrm{r}}\cdot\boldsymbol{\alpha}\Delta T\,\mathrm{d}V\\
&\quad = BL^{(k)}(\Delta T)^2\sum_i E_i^{(k)}\alpha_i^{(k)}\left\{\big(H^{(k)} - \alpha_i^{(k)}\big)t_i^{(k)} - \frac{F^{(k)}}{2}\big\{z_i^{(k)2} - z_{i-1}^{(k)2}\big\}\right\}\\
&\quad \equiv BL^{(k)}(\Delta T)^2 I^{(k)}
\end{aligned} \tag{12}$$

is derived in a straightforward manner. Here, $t_i^{(k)}$ is the thickness of each layer in the region k and $L^{(k)}$ is the length of each region; $L^{(1)} = L^{(2)} = a$, $L^{(3)} = L - a$. Therefore, the following equation is obtained.

$$\Delta G_b = \frac{(\Delta T)^2}{2}(I^{(1)} + I^{(2)} - I^{(3)}). \tag{13}$$

The substitution of equations (6), (7) and (13) into equation (4) results in

$$G = \frac{P^2}{2B}\left(C^{(1)}(a + \chi^{(1)}t^{(1)})^2 + C^{(2)}(a + \chi^{(2)}t^{(2)})^2\right) + \frac{P\Delta T}{B}(F^{(1)} - F^{(2)})a + \frac{(\Delta T)^2}{2}(I^{(1)} + I^{(2)} - I^{(3)}). \tag{14}$$

2.3. Relationship Between Apparent Fracture Toughness and True Fracture Toughness

The evaluated fracture toughness without consideration of any residual thermal stresses is calculated using the first term of equation (14), whereas the true fracture toughness including residual thermal stresses should be evaluated using the whole equation (14). Therefore, the relationship between the apparent fracture toughness without thermal stresses ($G_{\mathrm{C}}^{\mathrm{app}}$) and the true fracture toughness ($G_{\mathrm{C}}^{\mathrm{true}}$) is expressed as

$$G_{\mathrm{C}}^{\mathrm{true}} = G_{\mathrm{C}}^{\mathrm{app}} + \frac{P\Delta T}{B}(F^{(1)} - F^{(2)})a + \frac{(\Delta T)^2}{2}(I^{(1)} + I^{(2)} - I^{(3)}) \equiv G_{\mathrm{C}}^{\mathrm{app}} + \Delta G_{\mathrm{C}}. \tag{15}$$

The adhesive fracture toughness can be corrected using equation (15) with the measured apparent toughness (based on the compliance method, etc.), material properties, specimen geometries, applied load and crack length. As test standards and existing researches established the accurate methods for measuring apparent fracture toughness (without residual thermal stresses), the apparent toughness (or apparent energy release rate) is treated as a known value and the correction terms (the second and the third terms in equation (15)) are focused on in the following section.

3. Analysis and Discussions

3.1. Finite Element Analysis of DCB Specimens

The energy release rates associated with crack growth during DCB tests were calculated by finite element analysis, and the difference in energy release rates between the cases with and without consideration of residual thermal stresses is discussed. The model analyzed in this study is shown in Fig. 3, and specimen configurations (material and geometry) in each case are summarized in Table 1. In the case of FRP adherends, FRP layers were placed so that the fiber direction coincides with

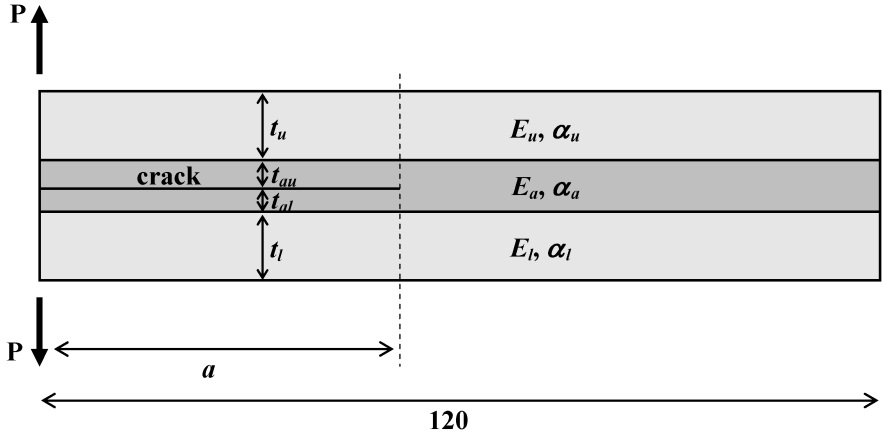

Figure 3. DCB specimen model.

Table 1.
Summary of the analysis model

	Case (1)	Case (2)	Case (3)	Case (4)	Case (5)
Upper adherend thickness t_u (mm) (material)	1.85 (FRP)	3.7 (FRP)	1.85 (FRP)	1.85 (FRP)	1.85 (FRP)
Upper adhesive thickness t_{au} (mm)	0.1	0.2	0.5	0	0.1
Lower adhesive thickness t_{al} (mm)	0.1	0.2	0.5	1.0	0.1
Lower adherend thickness t_l (mm) (material)	1.85 (FRP)	3.7 (FRP)	1.85 (FRP)	1.85 (FRP)	1.85 (Al)
Applied load P/B (N/mm)	2.19	6.05	2.33	2.33	2.15

Table 2.
Material properties used in the analysis

	Adherend (FRP)	Adherend (Al-alloy)	Adhesive
Young's modulus E (GPa)	L: 88.1 T: 28.6	77.1	9.65
Poisson's ratio ν	0.28	0.35	0.44
Shear modulus G (GPa)	10.8	28.6	3.35
CTE α (10^{-6}/°C]	L: 1.71 T: 11.8	15.6	26.0

the longitudinal direction of DCB specimens. The material properties used in this study were referred to reference [13] and are summarized in Table 2. In all cases, the applied loads were determined so that the energy release rate at a crack length of 60 mm was equal to 400 J/m^2 (see Table 1). The temperature change was set

to −280°C when including the residual thermal stresses in the analyses. ABAQUS Ver. 6.5 was used for calculation, and the DCB specimens were modeled as four-noded plane-stress isoparametric elements. The number of elements used was about 20 000. Note that plane stress elements corresponding to the beam assumption were used because the verification of the present correction method was the major concern in this section. The energy release rates were calculated using the virtual crack closure technique (VCCT). The total energy release rates are considered instead of investigating the mode separation or the phase angle of interfacial cracks.

3.2. Results and Discussions

3.2.1. Verification of the Present Correction Method

The calculated energy release rates are shown as a function of crack length in Figs 4–7 for the cases of (1)–(4). The FEM-based energy release rates without residual thermal stresses (G^{app}) are higher than those including residual thermal stresses (G^{true}). This result indicates that the evaluated fracture toughness without consideration of residual thermal stresses will be overestimated compared to the true fracture toughness. The correction values (ΔG) are calculated using the present method, and the energy release rates including residual thermal stresses are predicted by summing up the energy release rates from the FEM results without thermal stresses (G^{app}) and the correction values (ΔG). These predicted energy release rates ($G^{\text{app}} + \Delta G$) are also shown as circles in Figs 4–7. For all cases, the predicted values coincide well with the FEM results including residual thermal stresses (G^{true}) within 5% errors, which reveals the validity of the present correction method. Therefore, it is concluded that the true fracture toughness can be estimated

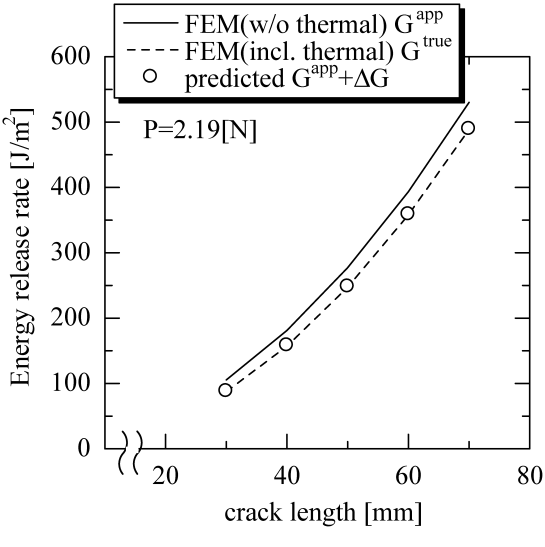

Figure 4. Comparison of the calculated energy release rate between the present correction method and FEM: case (1).

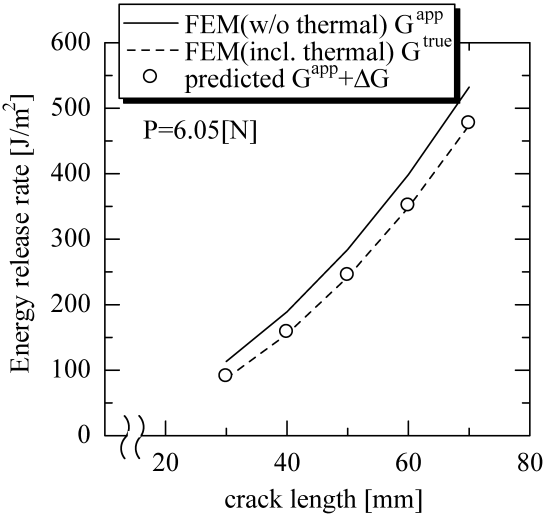

Figure 5. Comparison of the calculated energy release rate between the present correction method and FEM: case (2).

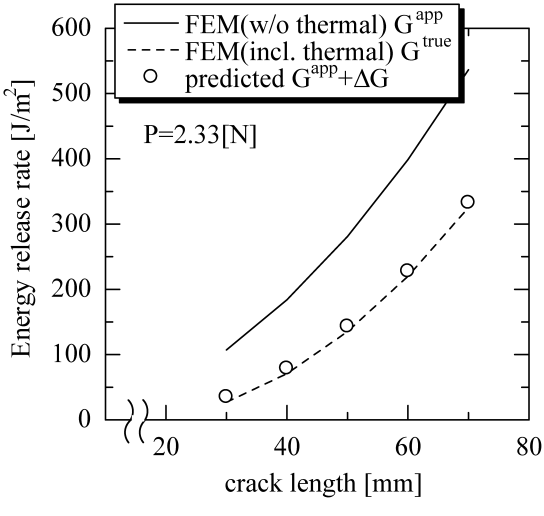

Figure 6. Comparison of the calculated energy release rate between the present correction method and FEM: case (3).

using the present correction method with the measured apparent fracture toughness (without consideration of residual thermal stresses).

Comparison of cases (1) and (2) indicates that the effect of residual thermal stresses on the energy release rates is significant when the total thickness of the specimen is large even in the cases of identical stiffness ratio and thickness ratio of the adherend and the adhesive. In addition, comparison of cases (1) and (3) reveals

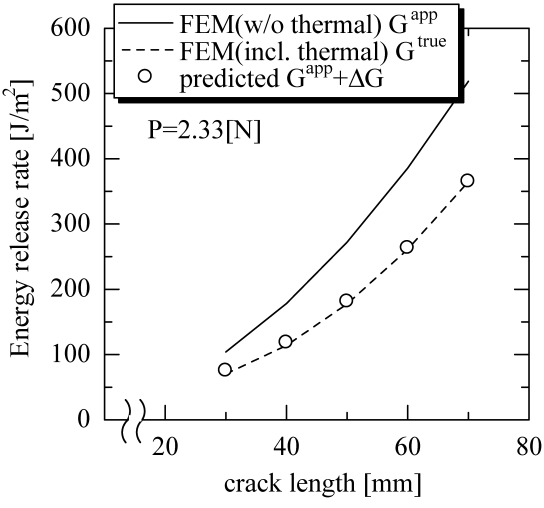

Figure 7. Comparison of the calculated energy release rate between the present correction method and FEM: case (4).

that an increase in adhesive thickness leads to an increase in the effect of residual thermal stresses on the evaluated energy release rates.

Effects of crack plane positions on the evaluated energy release rates can be investigated by comparing the cases (3) and (4). Case (3), in which the crack is located in the middle of adhesive layer, has a large difference between energy release rates including thermal stresses and those without thermal stresses compared to case (4), in which the crack is located at the interface between the adherend and the adhesive. However, the effect of crack plane positions is not significant in DCB specimens with thin adhesive layer such as case (1).

The calculated energy release rates as a function of crack length are shown in Fig. 8 for case (5), in which different adherends are bonded (i.e. asymmetric DCB specimen). In this case, the energy release rates including residual thermal stresses are higher than those without residual thermal stresses. Although the DCB specimen of case (5) has the identical geometry to that of case (1), the effect of residual thermal stresses on energy release rates is significant in case (5). The present correction method is also effective in the cases of unsymmetric DCB specimens.

The ratios of the corrected energy release rates using the present method ($G^{\text{app}} + \Delta G$) to the apparent energy release rates without consideration of thermal stresses ($G^{\text{app}} = 400$ J/m^2) are plotted as a function of temperature change in Fig. 9 when the crack length is equal to 60 mm in each case. Temperature dependence of material properties is neglected in this calculation. The difference between the apparent values and the corrected values becomes large due to the increase of temperature change, even in the cases of DCB specimens with thin adhesive layers (see cases (1) and (5)). Therefore, attention to the thermal stress effect is necessary for adhesive DCB tests, especially under cryogenic conditions, and the present

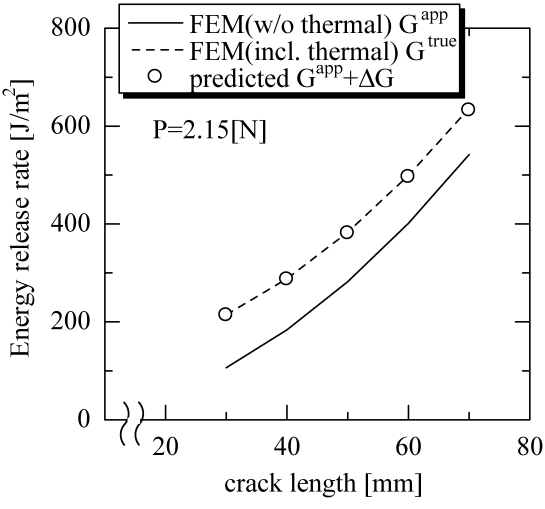

Figure 8. Comparison of the calculated energy release rate between the present correction method and FEM: case (5).

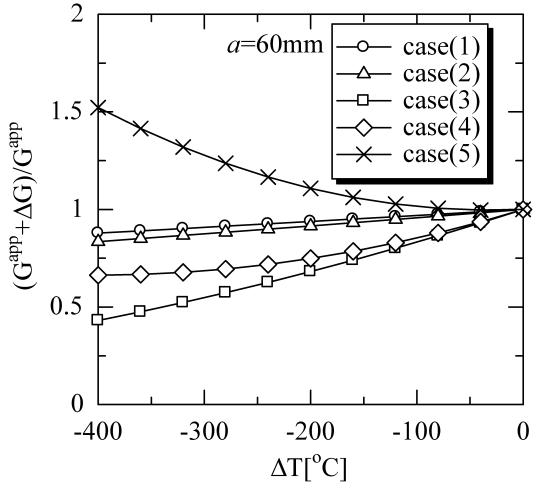

Figure 9. Relationship between temperature change and energy release rate ratio $((G^{\text{app}} + \Delta G)/G^{\text{app}})$.

correction method is considered to be effective for measuring accurate adhesive fracture toughnesses.

3.2.2. Relationship Between Crack Opening Displacement and Energy Release Rate

The relationship between crack opening displacement and energy release rate, which is considered to be one of the basic mechanisms as described in Section 1, is discussed. FEM results of case (1) at a crack length of 70 mm indicated that crack opening displacements (CODs) at the loading point were 11.69 mm for the

case without residual thermal stresses and 10.97 mm for the case including residual thermal stresses. This result shows that the cracked arms deform inside and COD decreases due to residual thermal stresses, which coincides with the decrease in energy release rate including residual thermal stresses (see Fig. 4). This tendency was observed in cases (1)–(4). The second term in the correction equation (14) or (15), which expresses the effect of COD change due to residual thermal stresses, was negative and significant compared to the third term within cases (1)–(4). Therefore, the above-mentioned relationship between crack opening displacement and energy release rate was observed.

On the other hand, FEM results of case (5) at a crack length of 70 mm indicated that CODs at the loading point were 12.11 mm for the case without residual thermal stresses and 11.61 mm for the case including residual thermal stresses. This result provokes the inference that the energy release rate including residual thermal stresses is smaller than that without thermal stresses. However, the opposite relation was recognized (see Fig. 8). In this case, the second term of the correction equation exhibited a negative value, which coincides with the result that COD including residual thermal stresses is smaller than that without residual thermal stresses. Nevertheless, the third term was positive and significant compared to the second term in case (5), and the energy release rate increased due to residual thermal stresses. Note that there is some possibility that the second term becomes significant depending on materials, geometries and applied loads. In the cases of asymmetric DCB specimens such as case (5), effects of energy release rates due to only temperature change (the third term in equation (14) or (15)) as well as the thermal deformation of the cracked arms (the second term in equation (14) or (15)) are important factors for the correction of fracture toughness.

In the cases of symmetric adhesive DCB specimens such as case (1), use of specimens with a thin adhesive layer or thick adherends results in the reduction of effects of thermal stresses on the evaluated fracture toughness (note that it is possible that adhesive performance may vary depending on the curing process variation due to thickness change). However, energy release rates due to residual thermal stresses cannot be generally neglected in the cases of asymmetric adhesive DCB specimens such as the case (5). When the thickness of the adherends increases, the energy release rates due to residual thermal stresses increase because of the scale effect. It is concluded that there are many cases that thermal stress correction to the fracture toughness evaluation is necessary in asymmetric DCB specimens. The optimization of the specimen configuration to minimize the effects of thermal stresses on the fracture toughness evaluation is further to be investigated.

4. Concluding Remarks

This paper described the necessity of correcting of residual thermal stresses to the fracture toughness evaluation using DCB, and an explicit formulation of the energy release rate was derived using a laminated beam model in the case of a general

DCB specimen with different adherends or crack in an asymmetric position. It was shown that the energy release rate is expressed as a summation of energy release rate associated with applied mechanical loads, that associated with the correction of COD due to thermal deformation, and that associated with only temperature change. The difference between the energy release rate including thermal stresses and that without thermal stresses was clarified, and a correction method was presented for the evaluation of the true adhesive fracture toughness. Energy release rates with and without consideration of thermal stresses were calculated using finite element analyses, and the effectiveness of the present correction method was verified by the comparison to the FEM results with the energy release rates corrected using the present method. The following statements are the conclusions obtained from the calculated results:

– The difference of the energy release rate with and without consideration of thermal stresses increase in the case of a thin adhesive layer or thick adherends.

– The corrected values of energy release rates including thermal stresses depend on the specimen geometry, material properties, crack length and the applied loads.

– The effects of thermal stresses on the correction of fracture toughness are significant when temperature change becomes large (e.g. cryogenic condition).

– The COD is correlated with the energy release rate in the cases of symmetric DCB specimens, and the corrected energy release rate is small compared to the apparent energy release rate when the cracked arms deforms inside due to residual thermal stresses.

– The effects of thermal stresses on the energy release rate is significant in the cases of asymmetric DCB specimens even when the adhesive layer is thin, and the energy release rate due to temperature change (the third term in the correction equation) as well as the effect of thermal deformation on the COD (the second term in the correction equation) should be considered for fracture toughness evaluation.

Acknowledgement

This study was conducted under the financial support of Grant-in-Aid for Scientific Research (No. 18760611).

References

1. M. J. Robinson, Composite cryogenic propellant tank development, *AIAA Paper 94-1375-CP* (1994).
2. T. Aoki, T. Ishikawa, H. Kumazawa and Y. Morino, Mechanical performance of CF/polymer composite laminates under cryogenic conditions, *AIAA Paper 2000-1605* (2000).

3. H. Kumazawa, T. Aoki and I. Susuki, Analysis and experiment of gas leakage through cross-ply laminates for propellant tanks, *AIAA J.* **41**, 2037–2044 (2003).
4. H. Suemasu, Y. Maeda and F. Namiki, Fracture mechanical study on initiation and growth of debonding between liner and FW layer of cryogenic composite material tank for rocket system, in: *Proc. 47th JSASS/JSME Struct. Conf.*, JSASS, Kanazawa, Japan, pp. 60–62 (2005).
5. J. He, T. Aoki and T. Shimoda, Cryogenic mode-II fracture behaviors of film adhesive in CFRP and aluminum bond joints, in: *Proc. 46th JSASS/JSME Struct. Conf.*, JSASS, Hachinohe, Japan, pp. 158–160 (2004).
6. J. He and T. Shimoda, Temperature-dependent fracture behavior of CFRP-film adhesive bond joints, in: *Proc. 29th JSCM Sympos. Compos. Mater.*, JSCM, Naha, Japan, pp. 163–164 (2004).
7. ASTM D3433-99, Standard test method for fracture strength in cleavage of adhesives in bonded metal joints, *Annual Book of ASTM Standards*. ASTM Philadelphia, USA (2005).
8. B. Blackman and A. Kinloch, Fracture tests on structural adhesive joints, in: *Fracture Mechanics Testing Methods for Polymers Adhesives and Composites*, D. R. Moore, A. Pavan and J. G. Williams (Eds), pp. 225–267. Elsevier, Amsterdam, The Netherlands (2001).
9. J. Jiao, C. K. Gurumurthy, E. J. Kramer, Y. Sha, C. Y. Hui and P. Borgesen, Measurement of interfacial fracture toughness under combined mechanical and thermal stresses, *J. Electron. Packag.* **120**, 349–353 (1998).
10. J. A. Nairn, Energy release rate analysis for adhesive and laminate double cantilever beam specimens emphasizing the effect of residual stresses, *Intl. J. Adhes. Adhes.* **20**, 59–70 (2000).
11. J. A. Nairn, Fracture mechanics of composites with residual thermal stresses, *J. Appl. Mech.* **64**, 804–810 (1997).
12. J. G. Williams, End corrections for orthotropic DCB specimens, *Compos. Sci. Technol.* **35**, 367–376 (1989).
13. R. Maruyama, T. Yokozeki, T. Ogasawara, T. Ishikawa and T. Ogawa, Study on the applicability of SiC-FRP to cryogenic tank structures with Al liner, in: *Proc. 2006 Ann. Mtg JSCM*, JSCM, Tokyo, Japan, pp. 137–138 (2006).

Appendix A. Derivation of Equation (3)

In the case of traction-free crack surfaces, the strain energy in equation (2) can be rewritten using equation (19) in reference [11] as

$$U = \frac{1}{2}\int_{S_T} \tilde{\mathbf{T}} \cdot \mathbf{u}^m \, dS + \frac{1}{2}\int_{S_u} \mathbf{T}^m \cdot \tilde{\mathbf{u}} \, dS + \int_{S_u} \mathbf{T}^r \cdot \tilde{\mathbf{u}} \, dS - \frac{1}{2}\int_V \boldsymbol{\sigma}^r \cdot \boldsymbol{\alpha} \Delta T \, dV, \tag{A.1}$$

where S_u denotes the displacement-prescribed area and $\tilde{\mathbf{u}}$ is the prescribed displacement vector on S_u. By substituting equations (A.1) and (2) into equation (1), the energy release rate can be expressed as

$$G = \frac{d}{dA}\left(\frac{1}{2}\int_{S_T} \tilde{\mathbf{T}} \cdot \mathbf{u}^m \, dS + \int_{S_T} \tilde{\mathbf{T}} \cdot \mathbf{u}^r \, dS - \frac{1}{2}\int_{S_u} \mathbf{T}^m \cdot \tilde{\mathbf{u}} \, dS - \int_{S_u} \mathbf{T}^r \cdot \tilde{\mathbf{u}} \, dS\right) + \frac{d}{dA}\left(\frac{1}{2}\int_V \boldsymbol{\sigma}^r \cdot \boldsymbol{\alpha} \Delta T \, dV\right). \tag{A.2}$$

Therefore, the energy release rate of the materials surrounded by only traction-loaded boundaries can be written as equation (3).

Appendix B. Derivation of Equations (5)–(8)

Displacement distributions in the longitudinal direction of the laminated beam can be expressed based on Bernoulli–Euler assumption as

$$u = u_0 - z\frac{\partial w_0}{\partial x}. \tag{B.1}$$

This distribution results in the following strain field;

$$\varepsilon_x = \varepsilon_0 + z\kappa, \tag{B.2}$$

where

$$\varepsilon_0 = \frac{\partial u_0}{\partial x}, \qquad \kappa = -\frac{\partial^2 w_0}{\partial x^2}. \tag{B.3}$$

In these equations, u_0 and w_0 are the displacements in the longitudinal and thickness directions, respectively, in the middle plane. The stress distribution in the beam can be expressed (including thermal strains) as

$$\sigma_i = E_i(\varepsilon_0 - \alpha_i \Delta T + z\kappa). \tag{B.4}$$

The application of lamination theory to the beam results in the following resultant stress/moment–strain/curvature relations.

$$\begin{aligned} N &= A_{11}\varepsilon_0 + B_{11}\kappa - N_{\mathrm{T}}\Delta T, \\ M &= B_{11}\varepsilon_0 + D_{11}\kappa - M_{\mathrm{T}}\Delta T. \end{aligned} \tag{B.5}$$

The constants (e.g. A_{11}) can be expressed in equation (8). The coordinates used are explained in Fig. 2. Although the following description corresponds to the region (1), similar equations can be obtained in the region (2).

In the case of a specimen with applied load P and without a temperature change, $N = 0$, $M = -Pa$ and $\Delta T = 0$ are substituted into equation (B.5), which results in

$$\varepsilon_0 = \frac{B_{11}}{A_{11}D_{11} - B_{11}^2}Pa, \qquad \kappa = -\frac{A_{11}}{A_{11}D_{11} - B_{11}^2}Pa. \tag{B.6}$$

Using equation (B.3),

$$\frac{\partial^2 w_0}{\partial x^2} = \frac{A_{11}}{A_{11}D_{11} - B_{11}^2}Pa \tag{B.7}$$

is obtained. Therefore, displacement at the loading point can be expressed as

$$w_0|_{x=a} = \delta^{\mathrm{m}} = \frac{1}{3}CPa^3. \tag{B.8}$$

On the other hand, in the case of a specimen with a temperature change and without an applied load, substitution $N = 0$ and $M = 0$ into equation (B.5) results in

$$\varepsilon_0 = \frac{D_{11}N_{\mathrm{T}} - B_{11}M_{\mathrm{T}}}{A_{11}D_{11} - B_{11}^2}\Delta T, \qquad \kappa = \frac{A_{11}M_{\mathrm{T}} - B_{11}N_{\mathrm{T}}}{A_{11}D_{11} - B_{11}^2}\Delta T. \tag{B.9}$$

Using equation (B.3),

$$\frac{\partial^2 w_0}{\partial x^2} = \frac{B_{11}N_{\mathrm{T}} - A_{11}M_{\mathrm{T}}}{A_{11}D_{11} - B_{11}^2}\Delta T \tag{B.10}$$

is obtained. Therefore, displacement at the loading point can be expressed as

$$w_0|_{x=a} = \delta^{\mathrm{r}} = \frac{1}{2}F\Delta T a^2. \tag{B.11}$$